PREPRINT UCRL-77073 Rev. 1

Lawrence Livermore Laboratory

LASER IRRADIATION OF PARYLENE DISKS WITH A 1.06 um LASER

R. A. Haas, D. W. Phillion, M. J. Boyle, H. N. Kornblum and V. C. Rupert

December 10, 1975

This paper was prepared for submission to the APS Meeting, St. Petersburg, Florida, November 10-14, 1975

LASER IRRADIATION OF PARYLENE DISKS WITH A 1.06 μm LASER

INTRODUCTION - (Vugraph 1)

Current interest in the laser driven compression and heating of matter has focused attention on; the physics of laser beam propagation and absorption in high temperature plasmas, the subsequent electron energy transport processes that transfer the absorbed laser energy to the high density ablation region and the resultant general convective fluid dynamic development of the heated plasma. This paper reports the results of a series of experiments performed with the Nd:YAG glass laser, Janus. The objective of these experiments was to use a relatively simple isolated target geometry to acquire basic data related to the previous questions. The results of a companion theoretical study will be reported in the following paper.[1]

To characterize each experiment as completely as possible, an extensive battery of laser and plasma diagnostics was employed. Emphasis was placed on determining; 1) the laser light energy balance[2] by measuring the angular distribution of scattered laser light with an array of photodiodes and an enclosing "box" calorimeter, 2) the time dependence of the incident and reflected laser light pulses, 3) the spatial[3] and energy distributions of the x-ray emission from the heated plasma and 4) the high energy electron[4] and ion emission[5] spectra.

To simplify the interpretation and evaluation of the experimental results 10 μm thick x 160 μm diameter parylene disks supported in vacuum

* This work was performed under the auspices of the U. S. Energy Research and Development Administration under contract W7405-Eng-48.

by slender glass stalks were irradiated. The 1.06 μm laser light was focused onto the target with an f/1.1 aspheric lens. The irradiation intensity level at the target surface was varied by changing the axial position of the target with respect to the focus of this lens. The nominal focal spot diameters at the target were 90, 30 and 10 μm. The face of the disk was always normal to the direction of propagation of the laser light. In order to minimize the effect of small scale self-focusing on the laser beam quality the laser was operated at focused powers $P \lesssim 100$ GW. In this regime of operation the B value[6] or phase delay at the beam center with respect to a low-intensity beam for Janus varies as $B(\text{waves}) \simeq 0.32 \times 10^{-2} P(\text{GW})$ and hence, was typically ~ 0.3 waves. The pulse length was varied from 50 to 100 psec. The irradiation flux levels on target were consequently in the 10^{15} to 10^{17} W/cm^2 range. Energy balance measurements indicate that 25-50% of the incident laser light was absorbed. The time integrated x-ray emission spectra, measured with a K-edge filter spectrometer, showed a two temperature behavior with a main body average energy of $\sim$ 0.5-1 keV and a high energy tail with an effective average of $\sim$ 10-30 keV. The corresponding high energy electron emission spectra, measured with a 90° focusing permanent magnet spectrometer with Si PIN detectors, had an average energy of $\sim$ 25-50 keV. X-ray microscope photographs of the plasma indicate that the low energy x-ray emission region is comparable in diameter to the laser light beam at the target and $\lesssim$ 10 μm thick in the direction of the laser beam. In the following, the optical diagnostics configuration, laser beam characteristics, target damage threshold and important results are discussed in more detail.

Vugraph #2

This vugraph shows the laser beam transport, focusing and optical diagnostics

system in the vicinity of the target chamber. The calorimeters measure the incident, reflected and transmitted laser light. The angular distribution of the scattered and reflected laser light was measured through 100 Å band-pass filters with photodiodes positioned in and perpendicular to the plane of polarization of the incident laser beam. The streak camera measured the temporal dependence of the incident and reflected laser light. The TV cameras were used to display the images of the front surface of the target and the incident laser beam at the target. The multiple image cameras rovided a calibrated measurement of the spatial distribution at the target of the backscattered and transmitted laser light.

Vugraph #3

High power target irradiation laser systems can emit enough low level radiation to alter the state of the target prior to arrival of the main laser pulse. Therefore, prior to performing experiments with a new class of target it is generally necessary to determine the damage threshold of the target. For the Janus laser system, premature energy emission comes from three sources: 1) amplified spontaneous emission (ASE) from the amplifier chain, 2) incompletely rejected pulses from the mode locked pulse train produced by the oscillator and 3) noise pulses switched out and amplified together with the main laser pulse. Items (2) and (3) will be referred to as pre-pulse damage. The possibility of ASE damage was checked by blocking the oscillator output and firing the laser system at a level that would normally produce a 250 GW output pulse. Close examination of the target revealed no observable damage. Using only the oscillator and preamplifiers, the prepulse damage threshold was determined to be ~ 4.5 J/cm^2.

This result is consistent with optical element damage thresholds.[8] An example of the target damage produced at 4.5 J/cm^2 is illustrated in this vugraph. At a 30 μm focal spot diameter this corresponds to ∿ 40 μJ of laser energy. The limit of detectability of the prepulse measurement system employed was typically ≳ 2-5 μJ. No evidence of significant prepulses was obtained for the experimental results reported here. However, for the highest intensities, ∿ 10^{17} W/cm^2, the detection capability of the system was comparable to the target damage threshold.

Vugraph #4

Characterization of a laser/plasma interaction experiment requires the measurement of the spatial and temporal dependence of the laser energy distribution at the target. For Janus the time integrated focused laser energy distribution, measured with a multiple image camera,[9] at two axial positions for a ∿ 160 GW focused laser pulse is shown in this vugraph. In the experiments reported here, the target was located at or near one of the axial positions documented in this vugraph. However, the laser output power was ∿ 100 GW and consequently, the small scale structure observed in these pictures was slightly less significant. Due to the astigmatism introduced by passage thru the disk amplifiers the beam was an elliptical shape. The average diameters of these distributions are 65-70 μm and 25-30 μm, respectively. The donut shaped structure is due to spherical aberration produced by whole beam self-focusing during amplification. The whole beam self-focusing produces a temporally dependent focal spot shift. In agreement with theory[9] the average shift is ∿ 5-7 μm at 160 GW and 3-5 μm at ∿ 100 GW. The data reported in this paper have been corrected

for this effect which is most significant for the high intensity, small focal spot diameter experiments. The large amplitude small scale structure observed in the beam at position number one is a consequence of small scale self-focusing of the beam as it passes thru the amplifiers. Since much of this structure begins early in the laser chain its amplitude is an exponential function of B and hence at $\sim$ 100 GW is a factor of $\sim$ 0.8 of the magnitude shown here. At position number two much of this structure has been smoothed by diffraction.

In the next vugraph the fraction of the incident laser energy backscattered thru the focusing lens is plotted as a function of the average peak intensity on target.

Vugraph #5

The fraction of incident laser energy backscattered, $\varepsilon_{BS}/\varepsilon_L$, decreases as the intensity, I_L, increases from $\sim 10^{15}$ W/cm^2 to $\sim 10^{17}$ W/cm^2. This, however, does not necessarily mean that a larger fraction of the incident laser energy was absorbed as the intensity was increased since the angular distribution of the scattered laser light was observed to vary with intensity as shown in the next vugraph.

Vugraph #6

The polarization averaged scattered laser light distribution, measured with the photodiode array, was generally highly peaked in the backscatter direction $\theta = 180°$. These distributions are consistent with classical refraction and stimulated backscatter. The fractions of the laser energy scattered in and perpendicular to the plane of polarization of the incident

laser beam were generally within a factor of two with more energy scattered into the perpendicular plane. This is consistent with the occurrence of some resonance absorption. The bars on this plot represent the standard deviation of the data at each nominal flux level. The $\sim 10^{15}$ W/cm^2 data are more highly peaked in the backscatter direction with less side scatter than the higher intensity, $\gtrsim 10^{16}$ W/cm^2, data. In particular, the fraction of the incident laser energy side scattered into the angular range $45° \leq \theta \leq 135°$ increased from $\sim$ 23 % at $\sim$ 100 GW/90 μm diameter $\sim 10^{15}$ W/cm^2 to $\sim$ 33% at $\sim$ 100 GW/30 μm diameter $\sim 10^{16}$ W/cm^2 to $\sim$ 39% at $\sim$ 100 GW/10 μm diameter $\sim 10^{17}$ W/cm^2. Since the convex curvature of the critical surface is probably increasing in these experiments it is not clear whether this is due to refraction, critical surface breakup or stimulated sidescatter. In the next vugraph the fraction of laser light absorbed and backscattered through the f/1.1 focusing lens is plotted as a function of the peak laser intensity.

Vugraph #7

From the plots shown in this vugraph it can be seen that according to the photodiode data, the fraction of laser light absorbed by the target plasma increases slightly with increasing laser intensity, I_L, as this parameter varies in the range 10^{15} W/cm$^2 \lesssim I_L \lesssim 10^{17}$ W/cm^2. However, the fraction absorbed remains nearly constant at $\sim$ 30% according to the "box" calorimeter data. The photodiodes and calorimeters are being carefully recalibrated to determine if this is the cause of the difference in the results of these two measurements. For this range of parameters the enhanced absorption, if it indeed occurs, is possibly due to one or a

combination of the following: sharp density gradients produced at the critical surface during resonance absorption, breakup of the critical surface into bubbles and tnen filaments within which enhanced absorption can occur and a decrease in the importance of Brillouim backscatter as a consequence of the limited mass and heat capacity of the underdense plasma. The latter explanation was first proposed by Kruer, Valeo and Estabrook[10], to explain time dependent reflectivity measurements made at the University of Rochester. This mechanism in which a reflection front propagates supersonically through the underdense plasma so that the reflection persists for a limited time $\tau_R \approx L[V_a(V_{os}/V_T)]^{-1}$, depends on the laser flux intensity and the plasma scale length L. In the formula for τ_R the ion acoustic velocity, electron thermal velocity and electron oscillatory velocity are denoted by V_a, V_T and V_{os}, respectively. For the irradiation and plasma conditions achieved in these experiments τ_R varies from $\sim$ 10 to $\gtrsim$ 50 psec as I_L varies from $\sim 10^{17}$ to 10^{15} W/cm^2. In the next vugraph measurements of the time dependences of the incident and reflected or backscattered laser light pulses are presented.

Vugraph #8

The reflectivity measurements presented in this vugraph are typical of those obtained in these experiments. An LLL ultrafast S-1 streak camera was used to monitor the time dependence of a thin strip across the center of the incident and backscattered laser radiation. The strip width was $\sim$ 5 to 10% of the width of each beam. A mirror pair with reflectivity 0.4 and 0.8 was placed in front of the streak camera so that several images, usually three, of each beam, reduced in intensity with respect to each

other by a factor of ~ 3, could be recorded simultaneously. In this vugraph two image sets are displayed for each intensity value. The differences are due to the fact that inaccuracies in the alignment of the different images prevent each from representing the same portion of the incident or reflected beam. Furthermore, since the temporal resolution of the streak camera was ~ 10 psec the very small scale structure can be interpreted as film and camera noise. It is, however, very likely that a high frequency substructure is present on the incident beam due to the random temporal dependence of small scale self-focusing events. The effect of this temporal structure on the results is not known. For incident laser fluxes of $\sim 10^{15}$ W/cm^2 the time dependence of the incident and backscattered laser light were very similar. However, for fluxes of $\sim 10^{16}$ W/cm^2 a significant difference was observed. As shown here, at $\sim 10^{16}$ W/cm^2 the reflected light pulse first increased rapidly reaching a maximum and then decreasing to a much smaller value just after the peak of the incident laser pulse. It is interesting to note that the characteristic time over which the large reflection is observed to occur is comparable to Kruer's characteristic time τ_R.

Vugraph #9

It is now well documented that the time integrated energy distributions of the x-rays emitted by laser produced plasmas do not generally satisfy a single "temperature" Boltzmann function. The corresponding results obtained in the present experiments are consistent with earlier observations. The low energy portion of the x-ray spectrum, 0.25 to 1.0 keV, was measured with a lead stearate bent crystal spectrometer loaded with Kodak Type 101

x-ray film. The x-ray spectrum above 1 keV was measured using a multi-channel K-edge filter spectrometer system. Using these diagnostics, the time integrated x-ray emission energy distribution has been measured over seven orders of magnitude in amplitude and three orders of magnitude in photon energy.

The low energy portion, 0.25 to 1.0 keV, of the x-ray emission spectrum, as shown here, was observed to increase in amplitude as the laser energy was increased. The emission minimum near 490 eV is believed to be due to the K-edge absorption of hydrogen-like carbon. It can also be seen from these data that as the incident laser flux was increased from 10^{15} to 10^{17} W/cm^2 the high energy tail of this distribution increased by two to three orders of magnitude. Measurements of the energy distribution of the high energy ($\geq$ 30 keV) electrons emitted by these plasmas were qualitatively consistent with these x-ray measurements. In particular, the number of high energy electrons emitted increased rapidly with increased incident laser high intensity. However, since the spatial and temporal dependence of the plasma potential was not measured it has not been possible to quantitatively relate the electron and x-ray emission spectra.

Vugraph #10

In addition to the x-ray energy distribution the spatial distribution of the x-ray emission was measured with an x-ray microscope. The x-ray microscope viewed the target from a position normal to the direction of the incident laser light. These measurements indicate that the characteristic dimensions of the x-ray emission region parallel to the axis of propagation

were $\sim$ 10 μm and remained essentially constant as the focal spot diameter was reduced. Also, as shown in the plot presented in this vugraph the FWHM diameter, D_x, of the x-ray emission region was generally less than the nominal FWHM diameter, D_L, of the laser beam for the $\sim$ 100 GW/90 μm diameter experiments. However, for the $\gtrsim$ 100 GW/30 μm diameter experiments the x-ray emission region was comparable to or greater than the laser beam focal spot diameter at the target.

Vugraph #11

Finally, in this vugraph results of ion emission measurements, obtained with Faraday ion collectors, are presented. The high energy tail of the ion distribution was observed to increase slightly with increased laser intensity. From this data it has been estimated that the fraction of the total ion emission energy carried away by ions with E/A $\gtrsim$ 10 keV increased from $\sim$ 0.5 $\pm$ 0.2 to $\sim$ 0.7 $\pm$ 0.2 as the experimental irradiation conditions were varied from $\sim$ 100 GW/90 μm diameter $\sim 10^{15}$ W/cm^2 to $\sim$ 100 GW/30 μm diameter $\sim 10^{16}$ W/cm^2. This variation, however, is probably within the uncertainty of these measurements.

Using an ion time of flight spectrometer[11] ultrahigh energy proton emission was also measured. It was found that the number and energy of the high energy protons emitted increased significantly as the laser flux was increased. At $\sim 10^{17}$ W/cm protons with energies $\lesssim$ 1 MeV were observed. The detailed regular structure observed in the spectrum shown here is very interesting and not understood at the present time. However, it clearly illustrates the danger inherent in assigning different charge and

mass states to peaks in Faraday collector measurements[12] of the charged particle emission from laser produced plasmas.

In summary, parylene disks supported on glass stalks have been irradiated with 1.06 μm wavelength laser light pulses focused to flux intensities in the range from 10^{15} to 10^{17} W/cm^2. According to photodiode measurements the fraction of laser light absorbed, 25-50%, increased slightly as the laser intensity was increased. However, "box" calorimeter measurements implied that the fraction absorbed was ~ 30% and insensitive to irradiation intensity. The error bars on both measurements are relatively large and this issue remains unresolved at the present time. Instrument calibrations are being rechecked to determine if this is the source of the discrepancy. The reflected laser light pulse exhibited a time dependence different from that of the incident pulse in the region of strong interaction, i.e., $I_L \sim 10^{16}$ W/cm^2. Consistent with the results of previous investigations, the number of high energy x-rays emitted by the plasma increased significantly with increased laser intensity. Furthermore, the diameter of the x-ray emitting region was comparable to the diameter of the laser energy distribution at the target surface.

REFERENCES

1. W. C. Mead, W. L. Kruer, J. D. Lindl and H. D. Shay, Bull. Am. Phys. Soc., 20, 1246 (1975).

2. D. W. Phillion, R. A. Lerche, V. C. Rupert, K. R. Manes, and S. R. Gunn, Bull. Am. Phys. Soc., 20, 1286 (1975).

3. M. J. Boyle, F. D. Seward, T. L. Harper, L. N. Koppel, K. J. Pettipiece, and H. G. Ahlstrom, Bull. Am. Phys. Soc., 20, 1348 (1975).

4. K. G. Tirsell, R. A. Haas, H. C. Catron, and V. W. Slivinsky, Bull. Am. Phys. Soc., 20, 1246 (1975).

5. V. C. Rupert, S. R. Gunn and J. F. Holzrichter, Bull. Am. Phys. Soc., 20, 1286 (1975).

6. J. A. Glaze, D. R. Speck and J. T. Hunt, "Geometrical Theory of Non-linear Phase Distortion of Intense Laser Beams," UCRL 76834 (1975).

7. D. R. Speck and D. MacQuigg (unpublished).

8. Alexander J. Glass and Arthur H. Guenther, Applied Optics 12, 637 (1973).

9. D. R. MacQuigg, J. F. Holzrichter, J. T. Hunt, J. E. Swain, D. R. Speck, E. Storm, K. J. Pettipiece, Bull. Am. Phys. Soc., 20, 1285 (1975).

10. W. L. Kruer, E. J. Valeo, and K. G. Estabrook, Phys. Rev. Lett., 35, 1076 (1975).

11. V. W. Slivinsky, H. G. Ahlstrom, K. G. Tirsell, J. Larsen, S. Glaros, G. Zimmerman and H. Shay, "Measurement of the Ion Temperature in Laser Driven Fusion," UCRL 78938 (1975).

12. A. W. Ehler, J. Appl. Phys., 46, 2464 (1975).

PARYLENE DISK IRRADIATION EXPERIMENTS – 1.06 μm

I. Objective: Use simple geometry to study laser/plasma interaction, plasma transport processes and fluid dynamics

II. Irradiation conditions:

Laser: $\left.\begin{matrix} \lesssim 5 - 15\ \text{J} \\ 50\text{–}150\ \text{psec} \end{matrix}\right\} < 100\ \text{GW output pulses}$

f1.1 focusing lens

10^{15}–10^{17} W/cm^2 on target

Target: Parylene disk

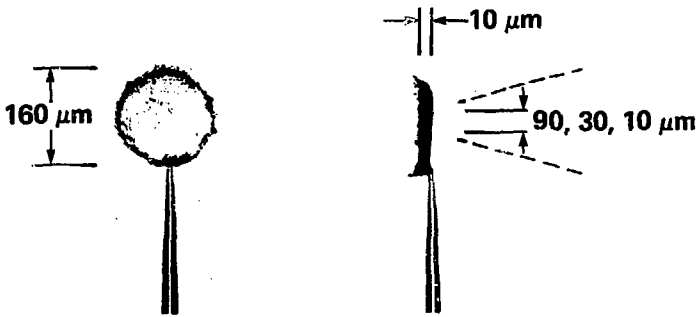

Vugraph #1

OPTICAL DIAGNOSTICS – 1.06 μm LASER/DISK EXPERIMENTS

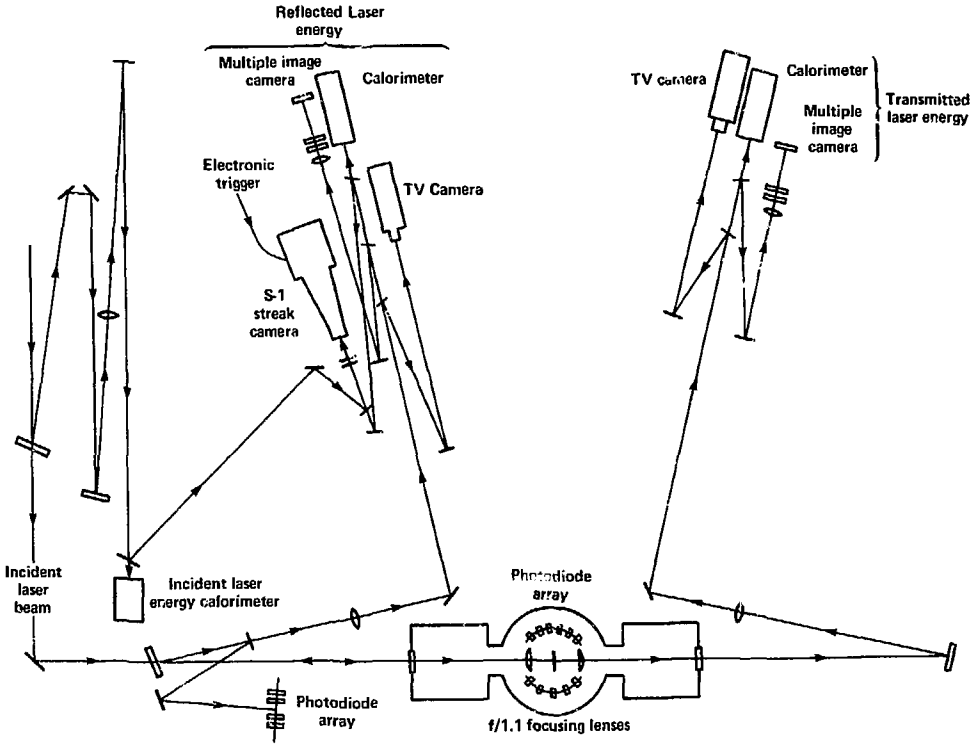

Vugraph #2

PARYLENE DISK TARGET DAMAGE CHARACTERISTICS – 1.06 μm LASER

~57 J/cm^2
60 psec
45 μJ/10 μm diam

~51 J/cm^2
54 psec
40 μJ/10 μm diam

~5.4 J/cm^2
62 psec
38 μJ/30 μm diam

30 μm

Local target damage
near threshold

1 μm

Vugraph #3

LASER ENERGY DISTRIBUTION ON TARGET – 1.06 μm LASER/DISK EXPERIMENTS

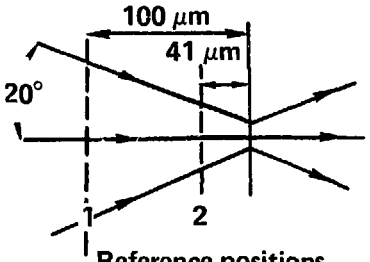

161 GW on target

— 10 μm wide scan
– – 5 μm wide scan

Reference positions

Reference position	Isoenergy contours	Horizontal scan	Vertical scan
1			
2			

⟷ denotes 10 μm

Vugraph #4

BACKSCATTERED LASER ENERGY FRACTION – 1.06 μm LASER/DISK EXPERIMENTS

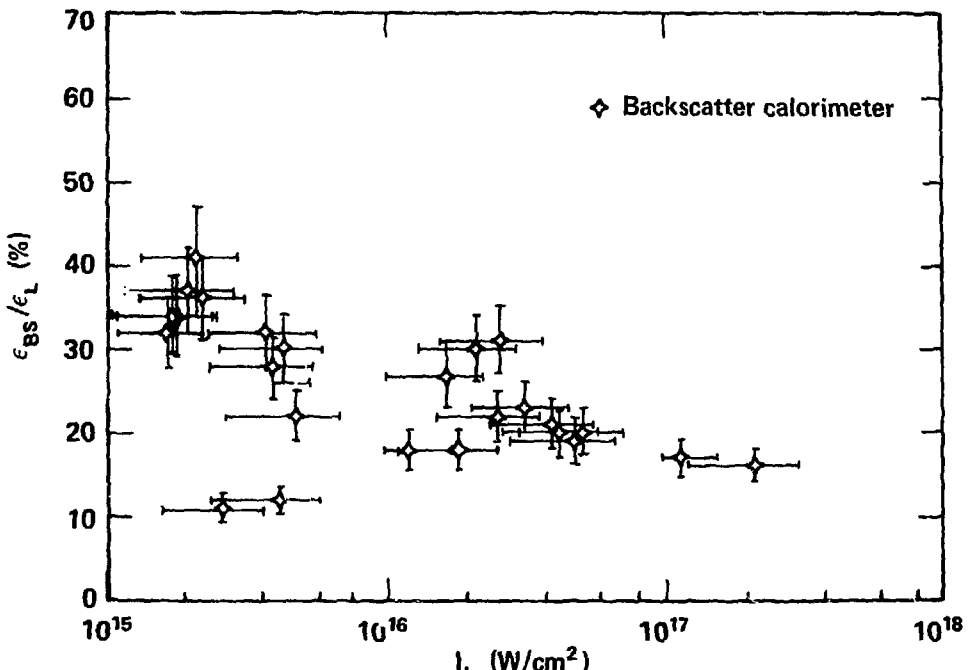

Vugraph #5

AVERAGED SCATTERED LASER LIGHT DISTRIBUTIONS – 1.06 μm LASER/DISK EXPERIMENTS

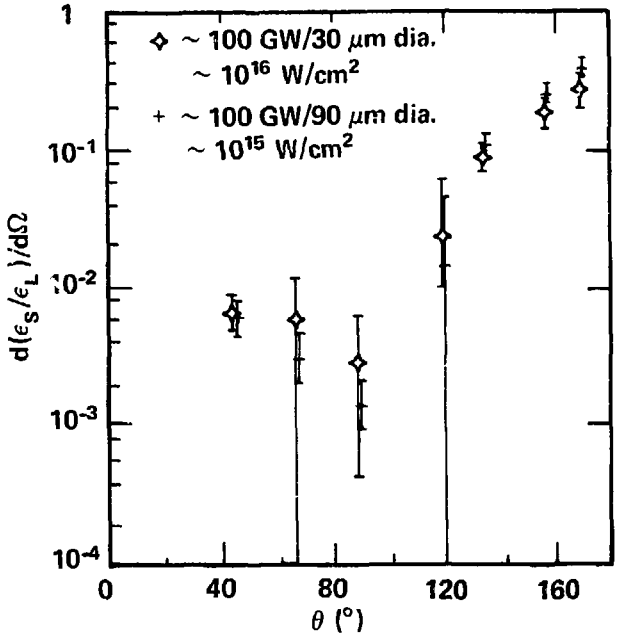

Vugraph #6

ABSORBED LASER ENERGY FRACTION – 1.06 μm LASER/DISC EXPERIMENTS

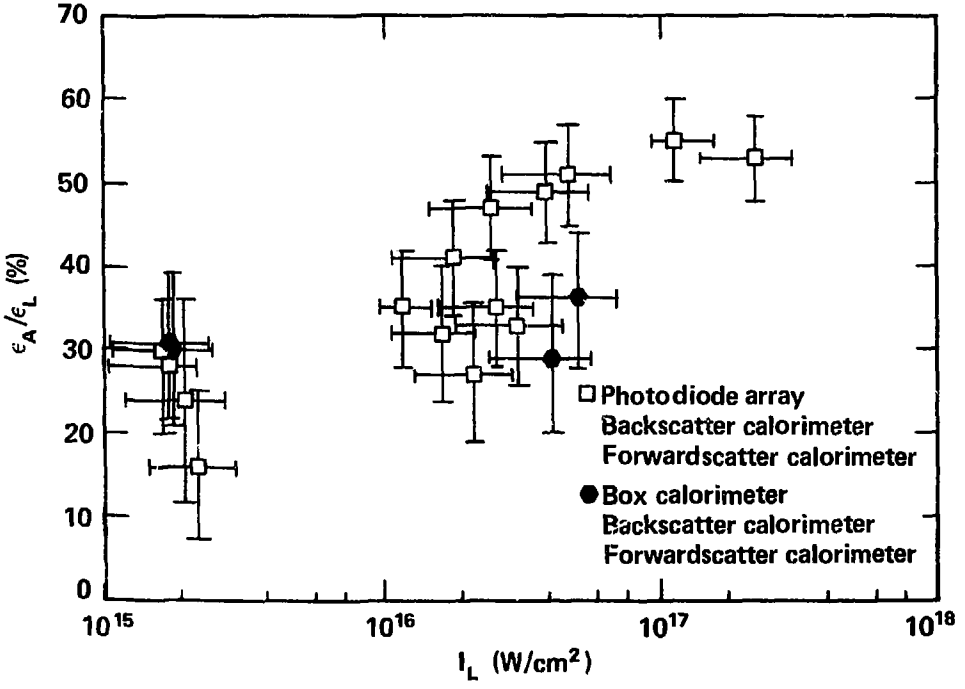

Vugraph #7

TEMPORAL DEPENDENCE OF BACKSCATTERED LASER LIGHT – 1.06 μm LASER/DISK EXPERIMENTS

Note: Incident (——) and Reflected (– – –) Pulses not plotted on same intensity scale.

$I_L \simeq 2.1 \times 10^{16}$ W/cm^2

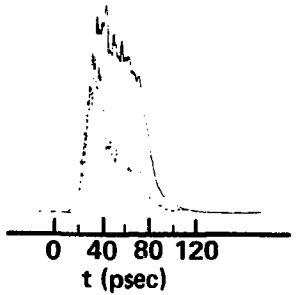

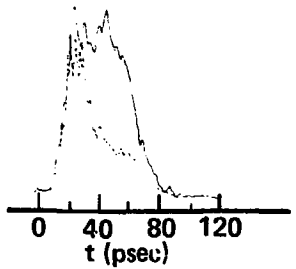

$I_L \simeq 2.5 \times 10^{16}$ W/cm^2

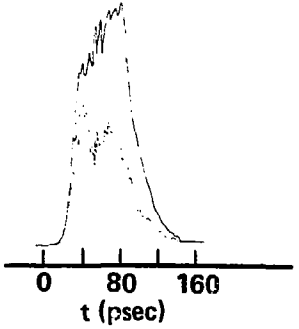

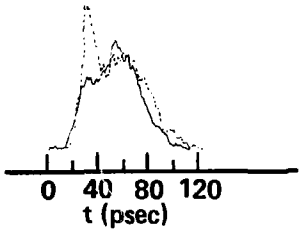

Vugraph #8

X-RAY EMISSION ENERGY DISTRIBUTIONS – 1.06 μm LASER/DISK EXPERIMENTS

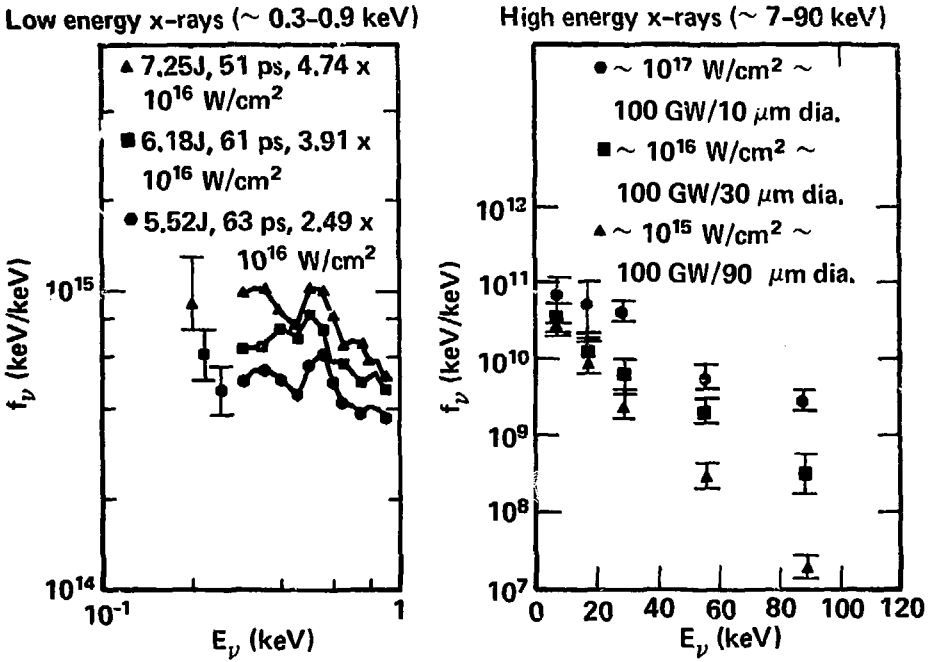

Vugraph #9

X-RAY EMISSION SPATIAL DISTRIBUTIONS – 1.06 μm LASER/DISK EXPERIMENTS

6.2J, 62 ps, 2.0 x 10^{15} W/cm²

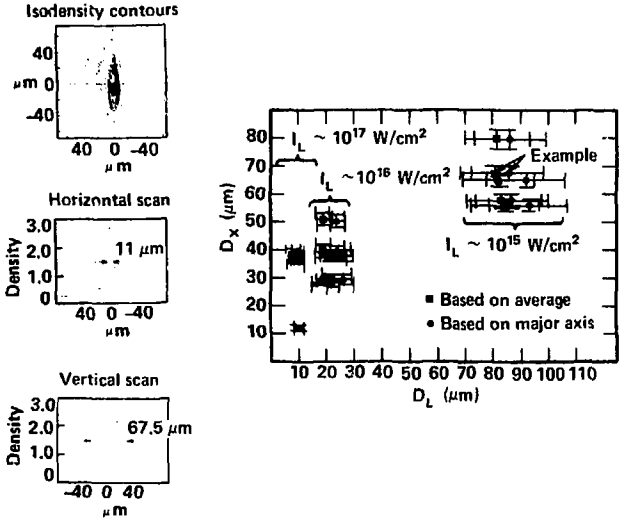

Vugraph #10

HIGH ENERGY ION EMISSION MEASUREMENTS – 1.06 μm LASER/DISK EXPERIMENTS

The fractional ion energy for E/A $\geqslant$ 10 keV increased with laser flux density on target

Averaged laser flux density	Fractional ion energy for E/A $\geqslant$ 10 keV
~100 GW/90 μm diam. ~10^{15} W/cm^2	0.5 ± 0.2
~100 GW/30 μm diam. ~10^{16} W/cm^2	0.7 ± 0.2

Ultrahigh energy proton emission increased with laser flux density on target, at ~10^{16} W/cm^2:

$\epsilon_{i_T} \lesssim 6.4$ mJ/sr

Resolution 2 keV

Detector distance 276.75 cm

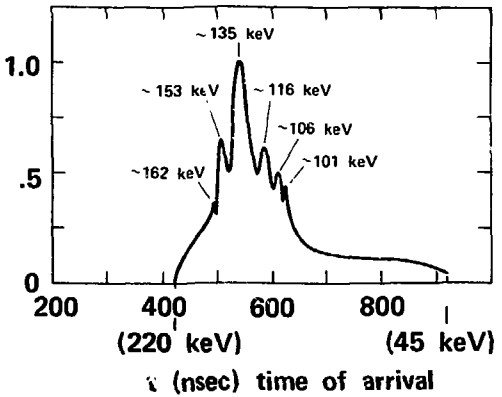

Vugraph #11